Effects of high pressure, high temperature and dilution on laminar burning velocities and Markstein lengths of iso-octane/air mixtures

ARTICLE *in* COMBUSTION AND FLAME · NOVEMBER 2012

Impact Factor: 3.08 · DOI: 10.1016/j.combustflame.2012.06.008

3 AUTHORS:

Bénédicte Galmiche
Imperial College London
8 PUBLICATIONS **79** CITATIONS
SEE PROFILE

Fabien Halter
Université d'Orléans
81 PUBLICATIONS **1,115** CITATIONS
SEE PROFILE

F. Foucher
Université d'Orléans
118 PUBLICATIONS **737** CITATIONS
SEE PROFILE

Combustion and Flame 159 (2012) 3286–3299

Contents lists available at SciVerse ScienceDirect

Combustion and Flame

journal homepage: www.elsevier.com/locate/combustflame

Effects of high pressure, high temperature and dilution on laminar burning velocities and Markstein lengths of iso-octane/air mixtures

Bénédicte Galmiche *, Fabien Halter, Fabrice Foucher

Laboratoire PRISME, Université d'Orléans, 8 rue Léonard de Vinci, 45072 Orléans Cedex 2, France

ARTICLE INFO

Article history:
Received 27 March 2012
Received in revised form 8 June 2012
Accepted 12 June 2012
Available online 1 August 2012

Keywords:
Iso-octane/air mixture
Nitrogen dilution
Oxygen enrichment
Laminar burning velocity
Markstein length

ABSTRACT

Spherically expanding flames are employed to measure flame velocities, from which are derived the corresponding laminar burning velocities at zero stretch rate. Iso-octane/air mixtures at initial temperatures between 323 and 473 K, and pressures between 1 and 10 bar, are studied over an extensive range of equivalence ratios, using a high-speed shadowgraph system. Effects of dilution are investigated with nitrogen and for several dilution percentages (from 5 to 25 vol% N_2). Over 270 experimental values have been obtained, providing an exhaustive data base for iso-octane/air combustion. Experimental results are in excellent agreement with recently published experimental data. An explicit correlation giving the laminar burning velocity from the initial pressure, the initial temperature, the dilution rate, and the equivalence ratio is finally proposed. Computed results using the two kinetic schemes and the Cantera code are compared to the present measurements. It is found that the mechanisms yield substantially higher values of laminar flame velocities than the present experimental results. Effects of oxygen enrichment are also investigated. A linear trend relating the percentage of oxygen in air and the unstretched laminar burning velocity is observed. Effects of high pressure, high temperature, and high dilution rate on Markstein lengths are also studied. As already done for the laminar burning velocity, an empirical correlation is proposed to describe the Markstein length for burned gases as a function of initial temperature and pressure, for equivalence ratios between 0.9 and 1.1, which has never been done before in the literature.

1. Introduction

Over the past decades, reducing the pollutant emissions and improving the fuel consumption of internal combustion engines have become hot topics. While much effort has been devoted to the development of electrically powered vehicles, internal combustion engines still remain the focus of a considerable amount of research.

Reducing CO_2 emissions requires simultaneous developments in different areas, which include vehicle dynamics and weight reduction, although most of the CO_2 reduction takes place through modifications in powertrain systems. The most important tool to reduce emissions with powertrain technologies is engine downsizing.

Gasoline engine downsizing is the process whereby the load operating point is shifted to a more efficient region through the reduction of engine capacity, while the full load performance is maintained via pressure charging. This has long been known as one of the most effective technologies for immediate implementation [1]. Further improvements in fuel economy have been shown to be possible through increased levels of engine downsizing [2]. However, many technical difficulties related to severe operating conditions (high pressure, high temperature, and high dilution rate) need to be overcome to achieve this high performance.

A thorough understanding of flame propagation under such conditions is essential for designing more efficient engines. Simulating downsized engines therefore requires the ability to accurately predict flame propagation at high pressure, high temperature, and high dilution rates. These simulations use turbulent burning models that require knowledge of the laminar burning velocity of the fuel-oxidizer mixture as a function of the unburned mixture temperature, pressure, and dilution rate. Indeed, laminar burning velocity is a widely used parameter describing the propagation of a one-dimensional, planar, adiabatic, premixed flame.

In the present study, iso-octane is used as a surrogate fuel for gasoline. This alkane molecule is a primary reference fuel and is widely used to understand combustion phenomena in spark ignition engines. However, experimental literature data still exhibit significant inconsistency in the iso-octane laminar burning velocities measured. A few studies have considered high-pressure flame propagation of iso-octane, such as the work by Metghalchi et al. [3], in which data for high pressure were extrapolated from low-pressure measurements, or the prior work by Gülder [4] and Jerzembeck et al. [5]. However, published data remain scarce and

* Corresponding author.
E-mail address: benedicte.galmiche@etu.univ-orleans.fr (B. Galmiche).

0010-2180/$ - see front matter © 2012 The Combustion Institute. Published by Elsevier Inc. All rights reserved.
http://dx.doi.org/10.1016/j.combustflame.2012.06.008

are not always consistent with one another. The spread of the measured values often exceeds the reported experimental uncertainty. Thus, there is a need for well-characterized and highly accurate fundamental experimental data for iso-octane.

The present study aims at constituting an exhaustive database of laminar burning velocities of iso-octane. The main goal of this study is to provide empirical correlations allowing the prediction of laminar burning velocity, over a wide range of temperature, pressure, equivalence ratio, nitrogen dilution rate, and oxygen enrichment rate. An empirical correlation to describe the Markstein length for burned gases as a function of initial temperature and pressure is also proposed.

2. Experimental setup

Experiments were carried out in a spherical stainless steel combustion chamber with an inner volume of 4.2 L (inner diameter 200 mm). A heater wire resistance located on the outer surface of the sphere was used to heat the initial gases to a maximum temperature of 473 K. Initial pressure inside the combustion chamber was limited to 10 bar.

The device is equipped with a vacuum pomp to achieve a residual pressure lower than 0.003 bar before the chamber is filled with the different gases. Synthetic air (79.5 vol% N_2 and 20.5 vol% O_2) was used for the experiments. Iso-octane was injected through a Coriolis mass flow meter (Bronkhorst mini CORI-FLOW 30 g/h) and the volumes of air and diluents were introduced with thermal flow meters (Brooks 5850S, 2 NL/min for air, and 0.5 NL/min for nitrogen). The injected air/diluent was directed to the exit of the Coriolis flow meter to convey the injected liquid. The inlet valve of the fuel/oxidant mixture was heated to 473 K to ensure the vaporization of iso-octane (vaporization temperature of 372 K at atmospheric pressure). To obtain a perfectly homogeneous premixed mixture a fan was installed inside the chamber to mix the gases. The fan is stopped 5 s before ignition in order to avoid any perturbation during the flame propagation experiments. A piezoelectric pressure transducer and a type-K thermocouple were used to check respectively the pressure level and the initial temperature before ignition. The maximum deviation between the effective initial pressure inside the combustion chamber and the required initial pressure was about 1%. The temperature fluctuation of the prepared mixture was within 2 K for the target initial temperature.

Two tungsten electrodes (diameter 1.5 mm), with a 1-mm gap, linked to a conventional capacitive discharge ignition system, were used for spark production at the center of the chamber. A larger gap between the electrodes provides more efficient ignition under lean conditions, but the electrodes must be fairly close to create and maintain the electric arc. In all experiments, the minimum discharge energy required for spherical flame initiation was supplied to the spark gap, in order to minimize the ignition-dominated phase [6]. To determine the minimum discharge energy, the charge time of the ignition coil was increased until spherical flame initiation. The minimum discharge energy was then deduced from the temporal measurements of the voltage and the intensity at the secondary winding of the ignition coil. This process was repeated for each operating condition. Depending on the initial pressure and temperature, the equivalence ratio, and the dilution rate, the discharge energy required for spherical flame initiation was varied between 25 and 51 mJ.

Two opposite and transparent windows (diameter 82 mm) provide optical access into the chamber. A LED illuminator (HardSoft DLR IL104G) equipped with an objective (HSO-PL-360) was used to provide continuous and incoherent light with a wavelength of 528 nm. A parallel light was created using a pinhole (diameter 3 mm), placed at the focal point of the objective, and a plano-convex lens (diameter 70 mm, focal length 1000 mm). After passing through the lens and the combustion chamber, the beam is displayed on a screen. The visualization of the flame was obtained using a classical shadowgraph method. Instantaneous images were recorded using a high-speed video camera (Photron Fastcam) operating at 6000 images per second. The temporal evolution of the expanding spherical flame was then analyzed. Figure 1 presents a schematic overview of the system.

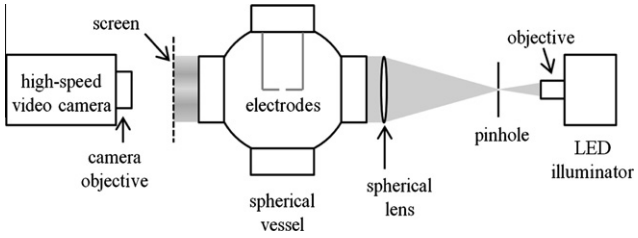

Fig. 1. Schematic overview of the system.

Measurements are limited to flames with diameters of 50 mm, corresponding to a volume of burned gases less than 1.6% of the chamber volume. Under this condition, the total chamber pressure can be considered constant during the initial stage of flame expansion. All the experimental values of laminar burning velocity reported in this paper are averages of three identical experiments. In the following, the mean value is presented.

3. Laminar burning velocity determination

After the spark, the flame front propagates spherically (Fig. 2). The instantaneous flame front radius was obtained from image postprocessing, after background subtraction. For each image, the luminous zone was fitted by a circle. The estimate of the circle radius and center is based on the minimization of the distance between the circle and luminous points. The temporal evolution of the flame front was obtained with the high-speed image recording. Only images corresponding to a flame front radius greater than 6.5 mm were used afterward in order to overcome ignition effects [7]. Then the laminar flame propagation velocity V_S^0 was deduced from the temporal evolution of the flame front radius r_f using a nonlinear methodology, which provides more accurate results [6,8]. This methodology is based on the nonlinear equation proposed by Kelley et al. [6],

$$\left(\frac{V_S}{V_S^0}\right)^2 \ln\left(\frac{V_S}{V_S^0}\right) = -\frac{L_b K}{V_S^0} \tag{1}$$

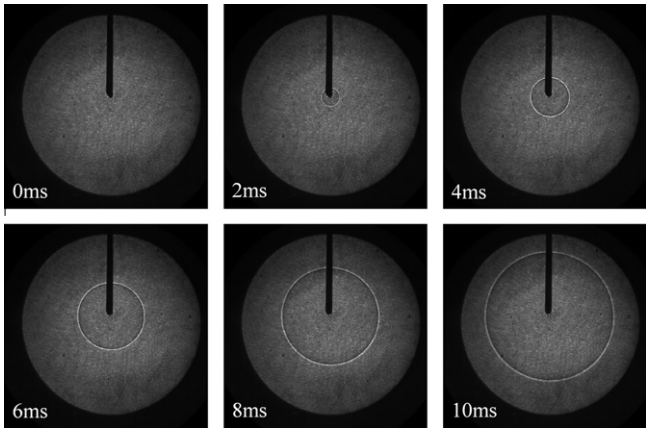

Fig. 2. Shadowgraph images of the propagating flame at different time delays after ignition (P_i = 1 bar, T_i = 423 K, ϕ = 1.0).

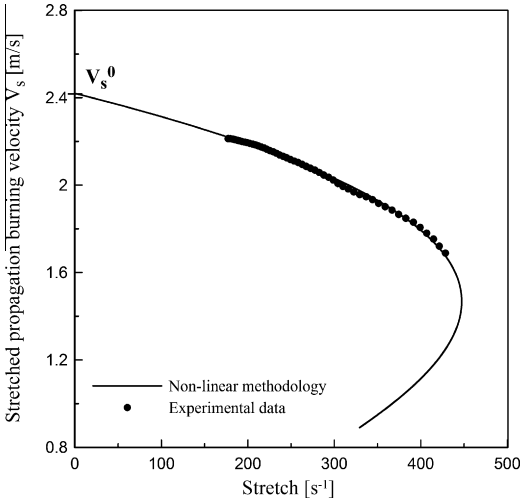

Fig. 3. Evolution of the stretched propagation velocity with stretch (iso-octane/air—equivalence ratio 0.8—P_i = 1 bar—T_i = 423 K).

where V_S is the stretched propagation flame velocity ($V_S = dr_f/dt$), V_S^0 the unstretched propagation flame velocity, L_b the Markstein length for burned gases, and K the total stretch acting on the flame.

The use of this nonlinear equation yields better results principally under fuel-lean conditions, where the burned gas Markstein length reaches or exceeds unity (in mm). These critical cases exhibit values of $\frac{S_b}{S_b^0}$ far from unity and so the linear methodology cannot be used with accuracy [8].

The stretch rate is defined as the temporal rate of change of a flame surface element of area A:

$$K = \frac{1}{A}\frac{dA}{dt} \tag{2}$$

In the case of a spherically expanding laminar flame, the total stretch acting on the flame is defined as

$$K = \frac{2}{r_f}\frac{dr_f}{dt} \tag{3}$$

The unstretched propagation flame velocity V_S^0 is then determined using the nonlinear extrapolation of the stretched propagation velocity V_S(K) (Fig. 3). The fundamental laminar burning velocity S_L^0 is finally obtained by taking into account the effects of the expansion factor [9],

$$\frac{V_S^0}{S_L^0} = \frac{\rho_u}{\rho_b} \tag{4}$$

where ρ_b and ρ_u are respectively the densities of burned and unburned gases computed using the EQUIL code from the Chemkin package developed at Sandia National Laboratories [10].

4. Numerical investigations

Numerical simulations were performed with Jerzembeck's et al. [5] and Hasse's et al. [11] kinetic schemes by solving the flat flame problem with Cantera software [12]. The Hasse et al. mechanism, comprising 48 reactions and 29 species, is based on the mechanism of Pitch et al. [13] but with three additional species (C_3H_6, N–C_3H_7, and I–C_3H_7). Jerzembeck et al. propose a high-temperature mechanism involving 99 species and 669 reactions.

Both slope and curve parameters are taken equal to 0.01, which induces about 1500 mesh points.

5. Experimental conditions investigated

In the first step, the laminar burning velocities of iso-octane/air mixtures were investigated for a wide range of conditions, without dilution. Five initial pressures and four initial temperatures were studied, over a variable range of equivalence ratios ϕ. Table 1 presents the conditions investigated.

For each pressure and temperature condition, the minimal equivalence ratio $\phi_{\min}$ corresponds to the limit of possible flame propagation for our ignition system. The upper limit in the equivalence ratio for which data are shown, $\phi_{\max}$, corresponds to the limitation of the image postprocessing. This limitation is due to the flame cellularity. Indeed, under fuel-rich conditions, the flame stability decreases and a cellular structure develops.

Among these different conditions, the case P_i = 1 bar/T_i = 423 K was chosen as the reference for the following study. In fact, the initial temperature T_i = 423 K is high enough to ensure complete vaporization of the fuel. The atmospheric pressure was chosen as the reference pressure.

In the second step, the impact of dilution on the laminar burning velocity was investigated for two initial temperatures and five initial pressures. Nitrogen was chosen as diluent with a dilution rate between 5 and 25 vol%. The level of dilution was increased as long as the combustion process remained energetic enough to ensure flame propagation; the maximum level of dilution depends on our ignition system. The combustion reaction follows the global one-step equation

$$\phi C_8H_{18} + 12.5(O_2 + 3.88N_2) + aN_2 \Rightarrow 8CO_2 + 9H_2O + (48.5 + a)N_2 + R$$

with R the quantity of excess air or unburned fuel for lean or rich mixtures, respectively.

The dilution rate τ is defined as the ratio between the diluent molar coefficient and the sum of the molar coefficients of the fresh gases:

$$\tau = \frac{a}{a + \phi + 12.5 \times (1 + 3.88)} = \frac{a}{a + \phi + 60.98}. \tag{5}$$

The conditions investigated with dilution are presented in Table 2. No flame propagation was observed at $T_i = 373$ K/$P_i = 1, 2, 3, 5, 10$ bar/$\tau = 25\%$ and $T_i = 423$ K/$P_i = 2, 3, 5, 10$ bar/$\tau = 25\%$ with the maximum possible discharge energy.

The effect of oxygen-enriched combustion was also examined. Reconstituted air from O_2 and N_2 was used for these experiments. Two different oxygen percentages (23 and 25 vol% O_2 in air) were investigated for the oxygen enrichment experiments. Experiments were conducted in the conditions previously defined as the reference: P_i = 1 bar and T_i = 423 K (see Table 3).

In the following graphs, each point represents the average of three identical experimental values. The standard deviation, corresponding to the scattering in experiments, is small: lower than 5% for the laminar burning velocity and lower than 0.3% for the equivalence ratio.

Table 1
Investigated equivalence ratios for iso-octane/air laminar burning velocity measurements, without dilution.

	1 bar	2 bar	3 bar	5 bar	10 bar
323 K	0.9–1.6	0.8–1.5	0.75–1.25	0.75–1.2	0.9–1.1
373 K	0.85–1.6	0.75–1.5	0.75–1.3	0.7–1.2	0.8–1.1
423 K	0.8–1.6	0.7–1.5	0.7–1.3	0.65–1.2	0.8–1.05
473 K	0.7–1.6	0.65–1.5	0.6–1.3	0.7–1.25	0.8–1.1

Table 2
Investigated equivalence ratios for iso-octane/air laminar burning velocity measurements, with addition of nitrogen.

Dilution rate (vol% N_2)		5%	10%	15%	20%	25%
373 K	1, 2, 3, 5 and 10 bar	1.1	1.1	1.1	1.1	–
423 K	1 bar	0.8–1.3	0.85–1.3	0.95–1.3	1.1–1.3	1.15–1.3
	2, 3, 5 and 10 bar	1.1	1.1	1.1	1.1	–

Table 3
Investigated equivalence ratios for iso-octane/air laminar burning velocity measurements, with addition of oxygen.

Percentage of oxygen in air	23%	25%
423 K – 1 bar	0.9–1.3	0.9–1.3

Equivalence ratio uncertainties can be evaluated based on the uncertainties of the gaseous volumes and on the liquid fuel mass injected. The flow controllers used for gaseous reactants possess an uncertainty lower than 1%: manufacturer data indicate an uncertainty of 0.7% in the flow rate and an additional uncertainty of 0.2% must be taken into account when flow meters are used in their full scale. Concerning the injected mass of iso-octane, the mass flow accuracy is better than 0.2%, as indicated in the manufacturer data. This leads to a global equivalence ratio uncertainty lower than 2%. Error bars are not shown in the different figures for reasons of clarity.

Uncertainty in the unstretched laminar burning velocity comes mainly from the fitting procedure of the temporal flame front radius evolution and from the extrapolation of the stretched propagation velocity to zero stretch. The global uncertainty in the unstretched laminar burning velocity can be estimated at ±5%.

6. Results and discussion

Laminar burning velocity is directly related to the reactive mixture properties and the thermodynamic conditions under which flame propagation takes place. Each of the parameters pressure, temperature, and dilution was independently investigated.

6.1. Effects of pressure and temperature

6.1.1. Experimental results

Experimental results are plotted in Fig. 4. Solid lines represent a new correlation detailed in the following section of the present paper.

As expected, for a fixed pressure, laminar burning velocity increases with temperature, since high temperatures boost the dissociation reactions that produce free radicals. These radicals initiate the combustion reaction, which is why the velocity of flame propagation increases [14]. Moreover, the density effect due to increased temperature also has to be considered. When the initial temperature is increased, the density of unburned gases is lower and so the density ratio ρ_u/ρ_b decreases. As an example, according to the density values computed using the EQUIL code from the Chemkin package, at $P_i = 1$ bar and $\phi = 1.0$, the densities of unburned and burned gases are respectively 1.12 and 0.151 kg/m^3 at $T_i = 323$ K and 0.768 and 0.145 kg/m^3 at $T_i = 473$ K. The density ratio is considered to evaluate the laminar burning velocity from the propagation velocity.

The increase in initial pressure at a fixed temperature leads to a decrease in the laminar burning velocity. At high pressures, the recombination reaction $H + O_2 + M \rightarrow HO_2 + M$ reduces the H atom concentration and thus competes with the initiation reaction producing free radicals O and OH: $H + O_2 \rightarrow O + OH$ [14]. This process tends to reduce the overall oxidation rate and to inhibit the combustion reaction. Thus the flame velocity decreases [14].

The lean and rich limits of the laminar burning velocity measurements depend on the initial pressure and temperature. In Fig. 4 (except for graph *e*), ϕ_{min} corresponds to the flame propagation limit for our ignition system. For lean mixtures, more experimental data can be obtained when initial pressure and temperature increase: at atmospheric pressure, the minimum equivalence ratio ϕ_{min} corresponding to an ignition success is about 0.90 at $T_i = 323$ K and 0.71 at $T_i = 473$ K. Indeed, the flammability of the lean mixtures is facilitated when the temperature of the fresh gases is high: in his study, Ternel [15] shows that the value of the minimum ignition energy decreases with increasing temperature. In other words, the energy needed to reach the initiation temperature of the combustion reaction is lower. At high initial pressure, reactive molecules are closer and ignition of lean mixtures is easier (graphs *b*, *c*, *d* in Fig. 4). At $T_i = 423$ K, the minimum possible equivalence ratio ϕ_{min} is about 0.82 at $P_i = 1$ bar and 0.65 at.$P_i = 5$ bar At $P_i = 10$ bar (graph *e*), initiation of the iso-octane/air mixture combustion is successful at equivalence ratios lower than those presented on this graph (However, the laminar burning velocities associated with these equivalence ratios are so low (between 10 and 20 cm/s) that the flame front is particularly distorted and the postprocessing of the shadowgraph images does not provide accurate results.

For fuel-rich mixtures, experiments were performed until flame cellularity was attained. The increase in initial pressure accentuates flame instabilities, so that the range of the measurements, in terms of equivalence ratios, decreases with increasing pressure: values of laminar burning velocities can be determined until $\phi_{max} = 1.61$ at atmospheric pressure, whereas the maximum equivalence ratio ϕ_{max} is 1.10 at $P_i = 10$ bar.

To validate our experimental setup and the methodology used to extrapolate the propagation flame velocity to zero stretch, the present results are compared with the recent experimental data of Kelley et al. [16]. In their study, they used the same method as in the present work (shadowgraph technique and nonlinear methodology for data postprocessing) to determine iso-octane/air laminar burning velocities. Their experiments were carried out at 353 K and at initial pressures between 1 and 10 bar. To compare our data with their results, a linear interpolation of our experimental data was conducted between 323 and 373 K. Results of this interpolation are plotted in Fig. 5.

For all the conditions investigated, the global trend is similar in the two studies, but a slight underestimation of our results is observed. This difference is related to the air composition used for the experiments. Indeed, in their experiments, Kelley et al. determine laminar burning velocities of iso-octane/air (21 vol% O_2, 79 vol% N_2) mixtures. In our study, the composition of air is 20.5 vol% O_2, 79.5 vol% N_2. To estimate the importance of the oxygen content on flame velocities, numerical simulations using the chemical kinetic scheme of Jerzembeck et al. [5] and the Cantera code [12] were conducted at 1 bar and 323 K, for two compositions of air. This analysis shows that a 0.5% increase in the oxygen content in air results in a 7% increase in the laminar burning velocity. This effect explains the slight difference observed between our results and those of Kelley et al. Thus this investigation shows that our measured data are in very good agreement with the latest study by Kelley et al. [16].

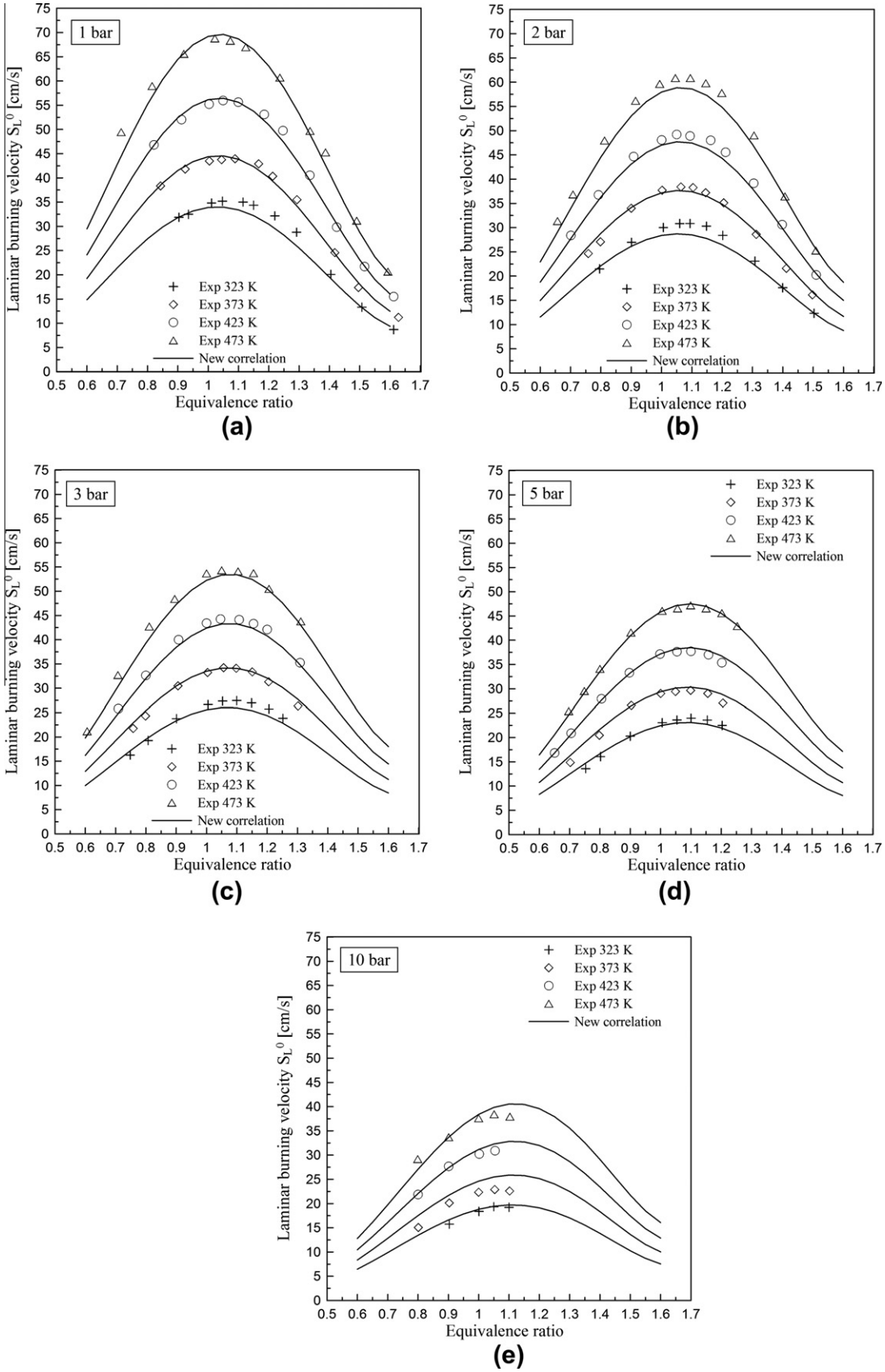

Fig. 4. Iso-octane/air laminar burning velocities at different initial pressure and temperature conditions (solid lines represent the new correlation (Eq. (6)) proposed in the present paper; the parameters of this correlation are presented in Table 4).

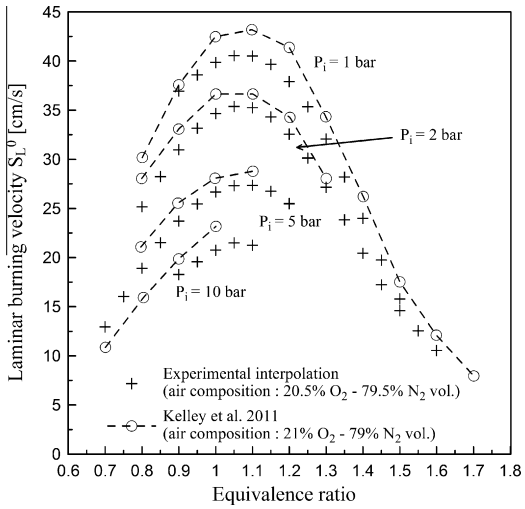

Fig. 5. Interpolation of the laminar burning velocities at T_i = 353 K and comparison with experimental results of Kelley et al. [16].

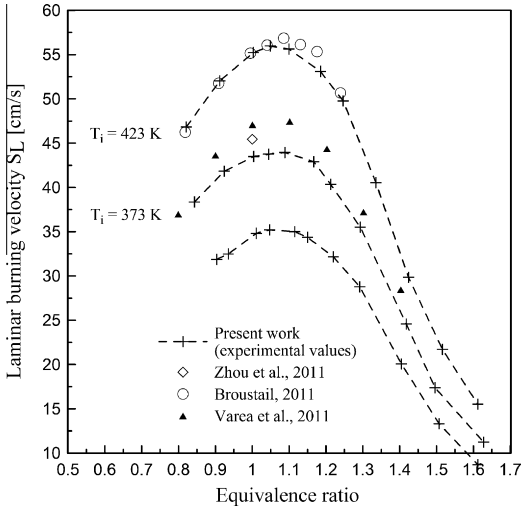

Fig. 6. Comparison with experimental results of Varea et al. [17], Zhou et al. [18], and Broustail [19] at P_i = 1 bar and T_i = 373 and 423 K.

Comparisons were also conducted with the experimental data of Varea et al. [17], Zhou et al. [18], and Broustail [19]. The results of these comparisons are plotted in Fig. 6. Excellent agreement is obtained with Broustail's results. As previously shown with the experimental results of Kelley et al., the difference between our results and those of Zhou et al. and Varea et al. is probably due to the air composition: in their experiments, Zhou et al. use reconstituted air with 21 vol% O_2 and 79 vol%. N_2, which results here in a 4% increase in the laminar burning velocity. Considering the air composition effect, these results are in very good agreement with our experimental data.

Both of these comparisons (Figs. 5 and 6) validate our experimental data over a wide range of pressures and several temperatures.

Our experimental results were also compared with different correlations [3,4,7,20–24] from the literature, approximating laminar burning velocity from initial pressure and temperature. Published data remain scarce and are not always consistent with one another (Fig. 7).

Empirical correlations have been obtained from the results of numerical simulations or from experimental measurements using different methods of laminar flame velocity determination. For example, Babkin et al. [20] and Metghalchi et al. [3] determined laminar burning velocities from the pressure rise of explosions in a spherical bomb. Figure 7 shows that there are significant discrepancies between all of these correlations. Nevertheless, good agreement can be observed between Metghalchi's correlation [3] and our experimental results, near stoichiometry and at low initial pressures. The difference at higher pressure (10 bar) is due to cellularity effects that are not detectable using the pressure recording technique and thus lead to overestimation in the determination of laminar burning velocities. The results of Gülder [4] are consistently higher that the present ones, as Gülder did not correct his measured flame propagation results to zero stretch. We can also see that the correlation proposed by Bradley et al. [7] is in quite good agreement with our experimental results presented in Fig. 7. However, Bradley et al. performed their experiments in a constant-volume chamber and postprocessed their extracted radius evolutions with the traditional linear methodology. The linear methodology has been shown to be inaccurate and to induce substantial errors below an equivalence ratio of 1 for iso-octane mixtures [8]. In all cases, the differences are mainly due to the different experimental setup and methodologies for data postprocessing, confirming that flame velocity measurement must still be improved.

Numerical simulations were performed with Jerzembeck's et al. [5] and Hasse's et al. [11] kinetic schemes. Figure 8 shows a comparison of the present experimental results and the predictions of the two mechanisms. As already observed in [16,18], although the overall trends are well predicted, Jerzembeck's kinetic scheme provides consistently higher values of laminar burning velocity than the experimental data. For Hasse's scheme, the laminar burning velocity values are lower than those of the experimental data in the case of a lean fuel mixture, whereas values higher than experimental data are obtained for rich fuel mixtures. Maximum laminar burning velocity is also shifted to richer fuel mixtures, while Jerzembeck's mechanism and our measured data show a maximum value at $\phi \sim 1.05$. These discrepancies confirm that iso-octane/air kinetic schemes still need to be improved.

Current published correlations and kinetic schemes for laminar iso-octane/air combustion are not consistent with one another or with the presented experimental results. Consequently, a new correlation is required, based on an extensive validated experimental database for a wide range of pressures, temperatures, and equivalence ratios. This is the aim of the following subsection.

6.1.2. Correlation

Using all of the experimental results under the operating conditions reported in Table 1, the laminar burning velocity evolutions, $S_L^0 = f(P_i, T_i, \phi)$, can be described by the relationship

$$S_L^0 = S_{L\mathrm{ref}}^0 \left(\frac{T_i}{T_{\mathrm{ref}}}\right)^{\alpha_s} \left(\frac{P_i}{P_{\mathrm{ref}}}\right)^{\beta_s} \tag{6}$$

where

$$S_{L\mathrm{ref}}^0 = A + B(\phi - \phi_m) + C(\phi - \phi_m)^2 + D(\phi - \phi_m)^3 + E(\phi - \phi_m)^4 \tag{7}$$

and

$$\alpha_S = \alpha_1 + \alpha_2(\phi - \phi_m)$$

$$\beta_S = \beta_1 + \beta_2(\phi - \phi_m)$$

P_{ref}, T_{ref} are respectively the reference pressure and temperature, and $S_{L\mathrm{ref}}^0$ is the unstretched laminar burning velocity for these conditions. In this correlation, pressures P_i and P_{ref} are expressed in bar, temperatures T_i and T_{ref} in K, and laminar burning velocities S_L^0 and $S_{L\mathrm{ref}}^0$ in cm s.

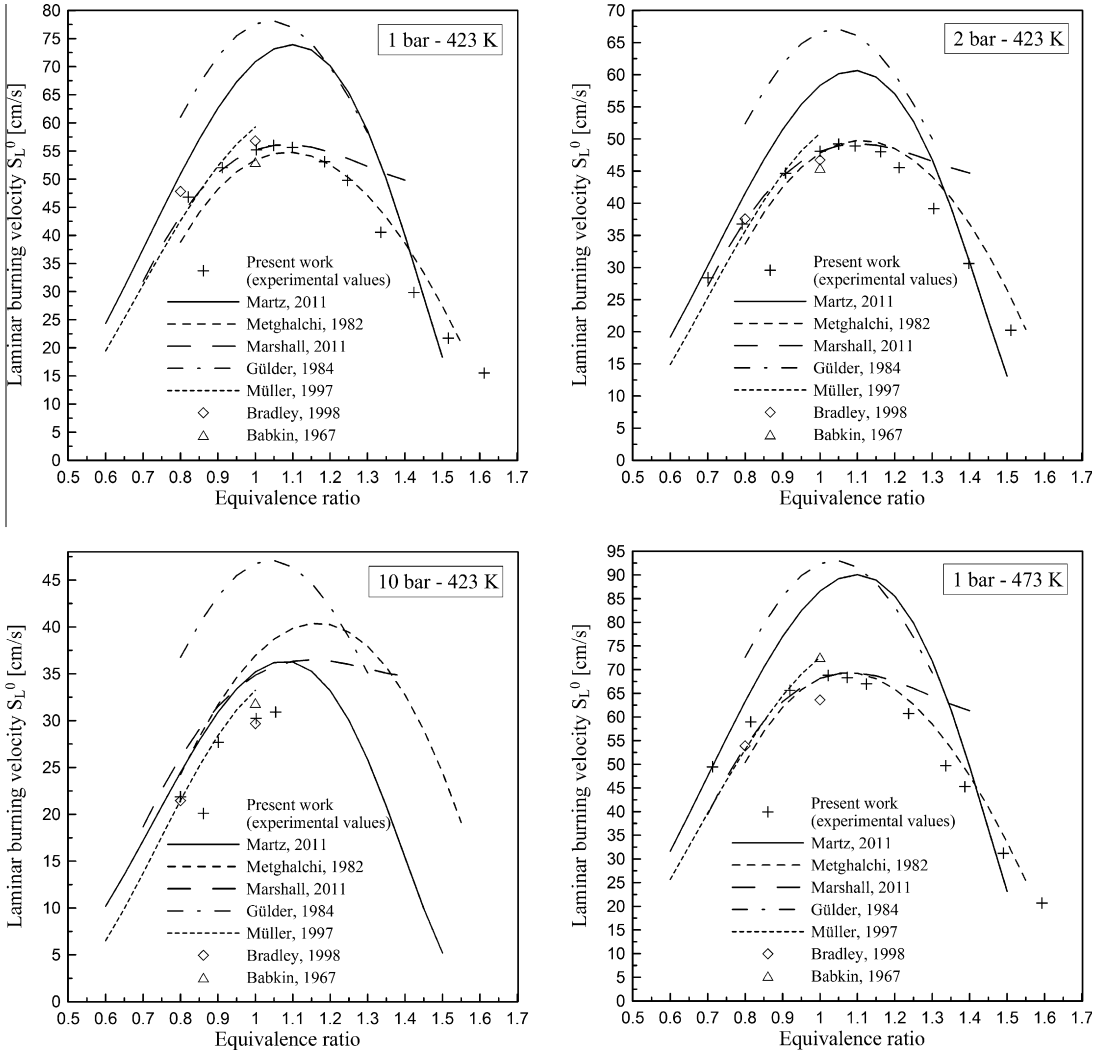

Fig. 7. Comparison of present results and literature correlations, for a few initial pressure and temperature conditions.

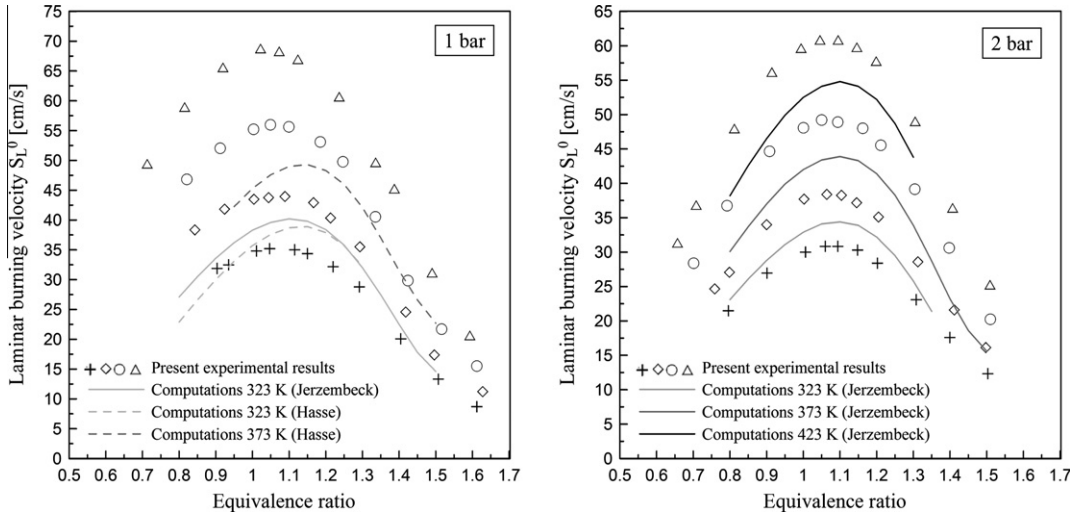

Fig. 8. Laminar burning velocity of iso-octane/air (crosses: T_i = 323 K, diamonds: T_i = 373 K, circles: T_i = 423 K, triangles: T_i = 473 K, dashed lines: Hasse's mechanism, solid lines: Jerzembeck's mechanism).

Table 4
Numerical values of the parameters in Eqs. (6) and (9).

Parameter	Optimized value
A	56.21
B	−14.44
C	−214.08
D	43.47
E	267.17
α_1	1.88
α_2	−0.19
β_1	−0.24
β_2	0.27
γ_1	2.67
γ_2	0.17
ϕ_m	1.07

All of the constant values A, B, C, D, E, α_1, α_2, β_1, β_2, and ϕ_m were optimized by minimizing the mean squared error between the experimental data and the correlation Eq. (6). Numerical values of the optimized parameters are presented in Table 4. This optimization is conducted in two steps:

- first, the parameters of Eq. (7) were optimized using the experimental data at $P_i = 1$ bar and $T_i = 423$ K,
- second, the parameters α_1, α_2, β_1, and β_2 were optimized using the experimental values of laminar burning velocity at initial pressures of 2, 3, 5, and 10 bar, and initial temperatures of 323, 373, and 473 K.

The global correlation Eq. (6) is plotted in Fig. 4. The average relative error between experimental data and this correlation is less than 3%.

This new correlation is now compared in Fig. 9 with numerous recently published experimental results [5,7,8,16–18,25–30]. The effects of initial temperature and initial pressure are displayed respectively in graph (a) and graph (b). Experimental data are in good agreement with the present correlation, considering the small differences in initial temperature between all the studies (effective initial temperatures are specified in the legends of both graphs) and the possible differences in the air composition and in the methodology used to extract the unstretched laminar burning velocity.

6.2. Effects of dilution

6.2.1. Results

The effect of nitrogen dilution on laminar burning velocity was investigated for the operating conditions presented in Table 2. All of the experimental results are plotted in Figs. 10 and 11 (solid lines represent a new correlation detailed in the following section of the present paper). As expected, laminar burning velocities decrease when the dilution rate increases: the N_2 dilution of the reactive mixture induces a diminution of the combustion temperature and therefore leads to a decrease in the laminar burning velocity.

The effect of oxygen-enriched combustion was also examined. Experimental values of the laminar burning velocity at the stoichiometric equivalence ratio versus the oxygen percentage in air are plotted in Fig. 12. Previous results concerning N_2 dilution are also presented in this figure. In these previous experiments, synthetic air (79.5 vol% N_2 and 20.5 vol% O_2) was used and nitrogen was used as diluent. In order to compare the N_2 dilution experiments to the O_2 enrichment experiments, the initial N_2-diluted mixture can be characterized by the quantity of oxygen, instead of the N_2 dilution rate as defined in the previous part. The percentage υ_{O_2} of oxygen in the global mixture of synthetic air and N_2 diluent is then defined as

$$\upsilon_{O_2} = \frac{n_{O_2(\text{synthetic air})}}{n_{O_2(\text{synthetic air})} + n_{N_2(\text{synthetic air})} + n_{N_2(\text{diluent})}} \times 100 \tag{8}$$

As already observed by Zhou et al. [18], it can be seen in Fig. 12 that the laminar burning velocity at stoichiometric equivalence ratio increases linearly with the increase in the percentage of O_2. This linear trend is confirmed by the predictions of Jerzembeck's and Hasse's schemes [18].

6.2.2. Correlation

An empirical term can then be added to the previous correlation (Eq. (6)) to take into account the effect of dilution,

$$S_L^0(\upsilon_{O_2}) = S_L^0(\upsilon_{O_2\text{ref}})\left(\frac{\upsilon_{O_2}}{\upsilon_{O_2\text{ref}}}\right)^{\gamma} \tag{9}$$

where $\gamma = \gamma_1 + \gamma_2(\phi - \phi_m)$, γ_1 and γ_2 are two constant values, υ_{O_2} is the percentage of oxygen in air defined by Eq. (8) $\upsilon_{O_2\text{ref}}$, is the reference percentage of oxygen in air and corresponds to the percentage of oxygen in the synthetic air used in these experiments,

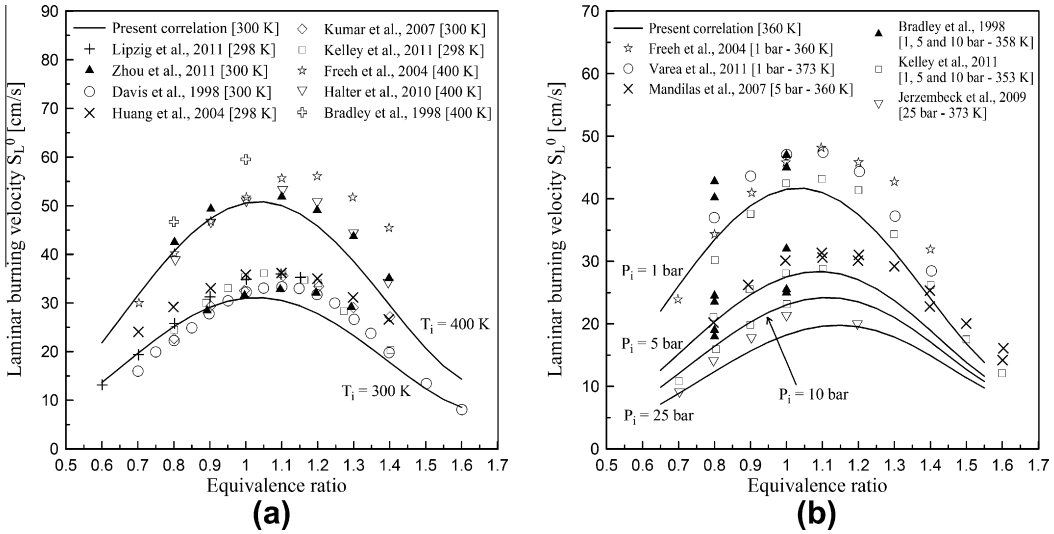

Fig. 9. Comparison between published experimental data and calculated results from the present correlation (Eq. (6)) at $P_i = 1$ bar (graph a) and $T_i = 360$ K (graph b).

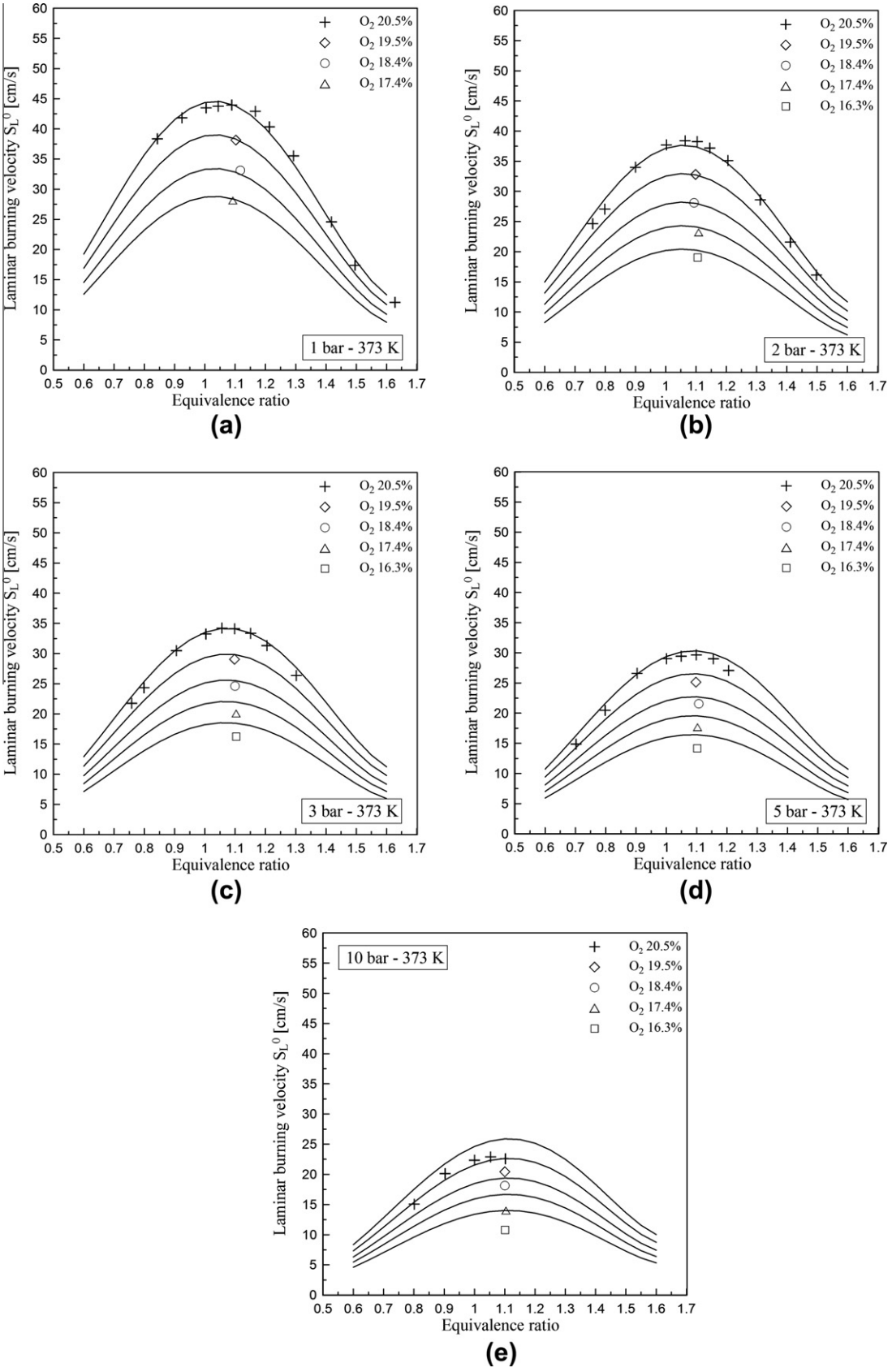

Fig. 10. Experimental results (symbols) and correlation (lines) for iso-octane/air mixtures evaluated at different initial pressures and different percentages of oxygen in air (T_i = 373 K).

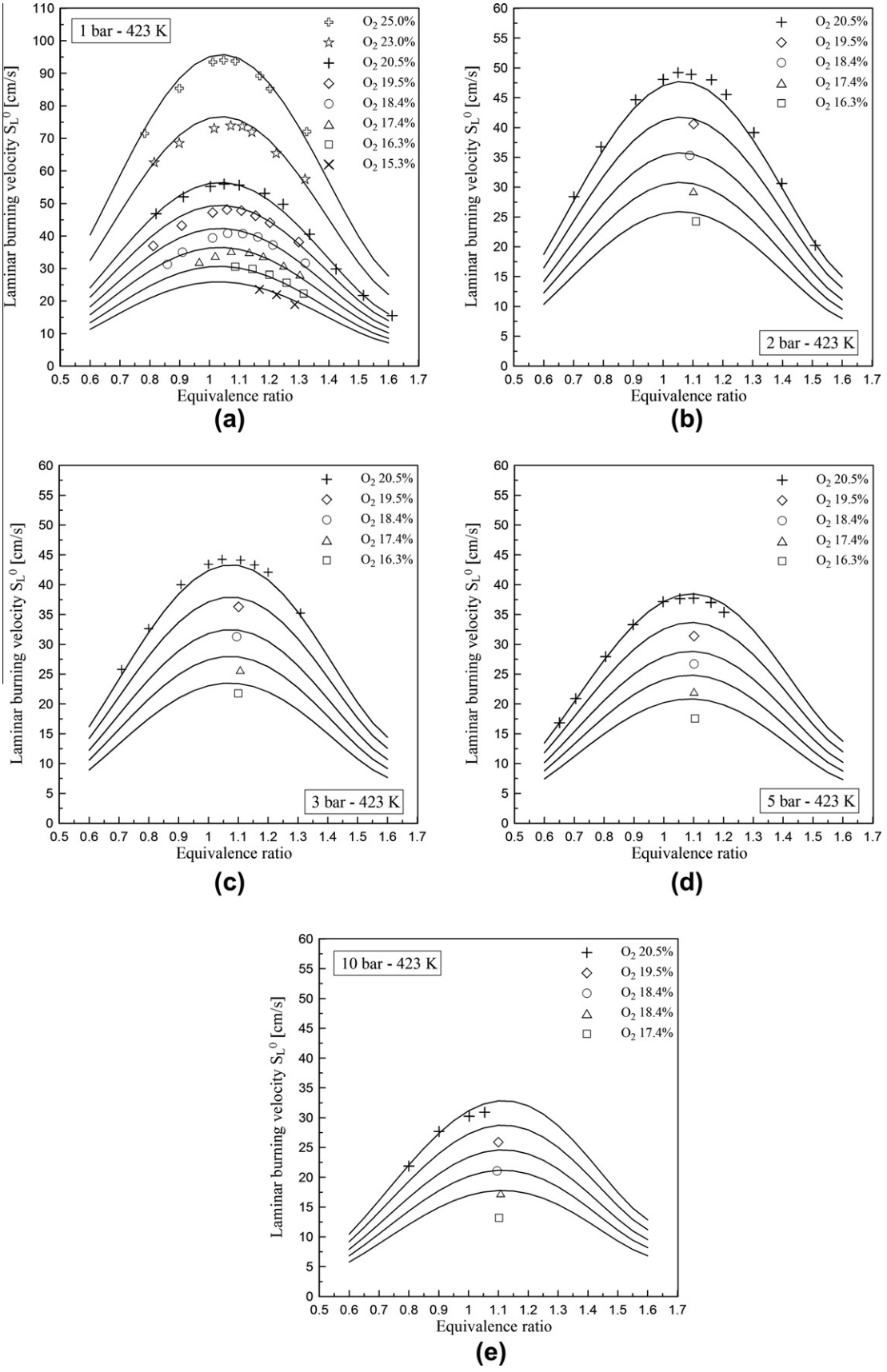

Fig. 11. Experimental results (symbols) and correlations (lines) for iso-octane/air mixtures evaluated at different initial pressures and different percentages of oxygen in air (T_i = 423 K).

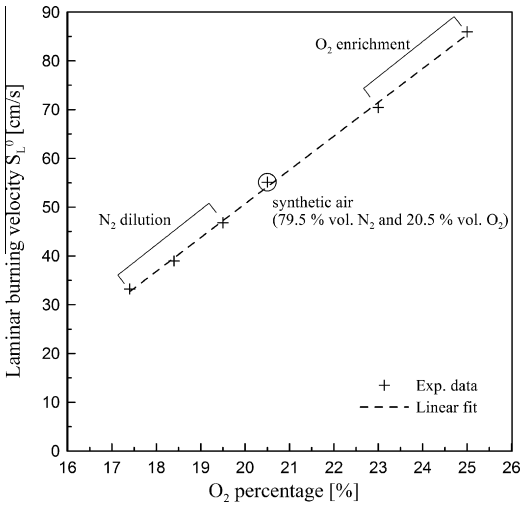

Fig. 12. Laminar burning velocities versus O_2 percentage in air, at stoichiometric equivalence ratio (P_i = 1 bar, T_i = 423 K).

$\upsilon_{O_2 ref} = 20.5\%$, $S_L^0(\upsilon_{O_2 ref}$ is the iso-octane/air laminar burning velocity expressed by the previous correlation Eq. (6).

The values of the two parameters γ_1 and γ_2 are optimized from the experimental data obtained with N_2 dilution and O_2 enrichment at the reference conditions 1 bar—423 K. Numerical values of the optimized parameters are presented in Table 4. This new correlation was then validated with the other data (T_i = 373 K and P_i = 1, 2, 3 and 10 bar). Very good agreement is observed (Figs. 10 and 11). The average relative error between experimental data and this correlation is less than 5%.

Table 5
Numerical values of the parameters in Eqs. (10) and (11).

Parameter	Optimized value
M	−1.74
N	2.50
α_L	−0.86
β_L	−0.79

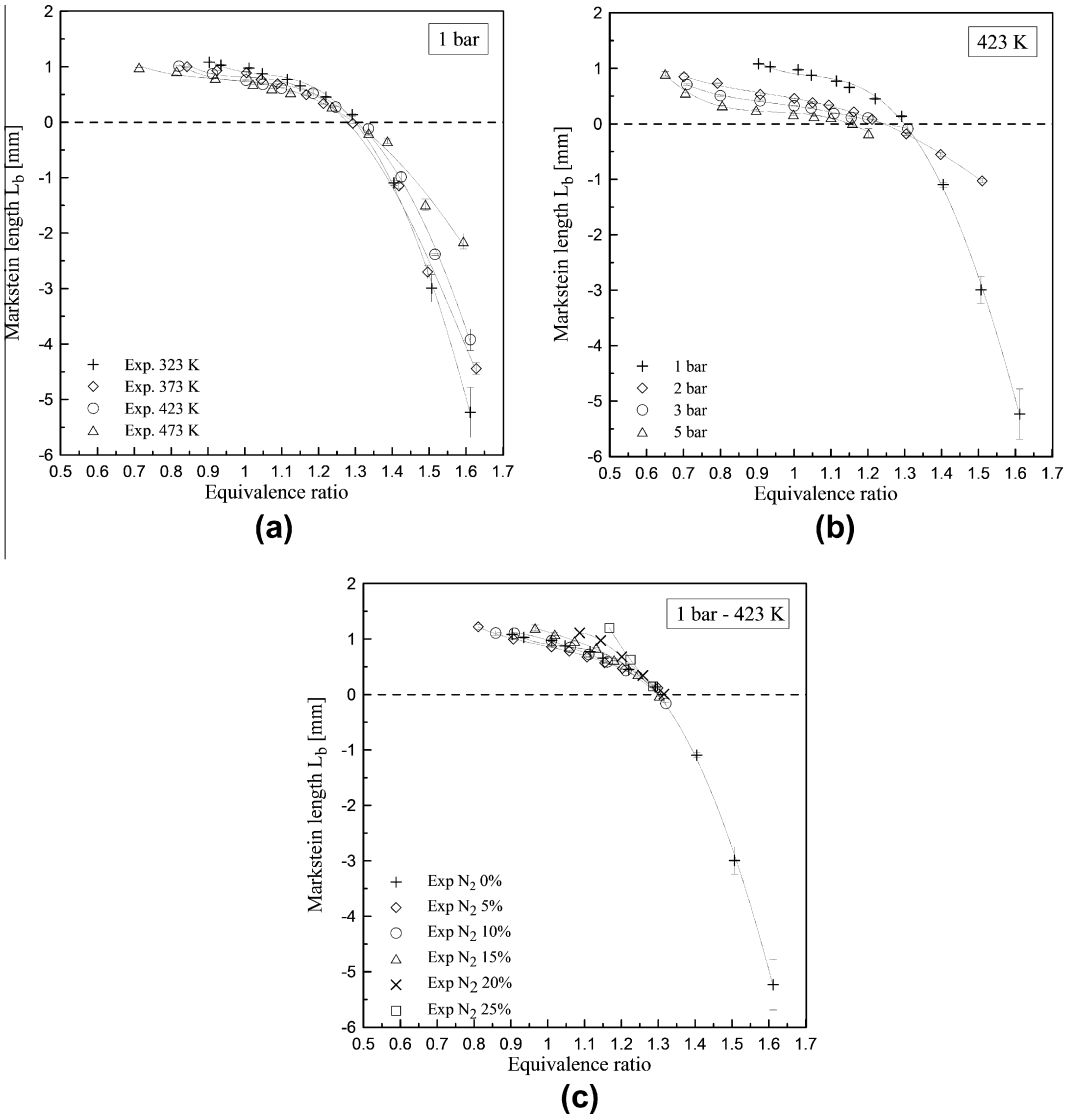

Fig. 13. Effect of initial temperature (a), initial pressure (b), and dilution rate (c) on the Markstein length for burned gases (the error bars correspond to the standard deviations).

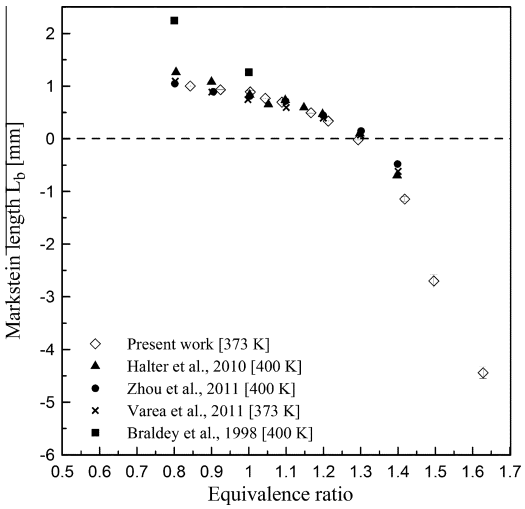

Fig. 14. Comparisons of present experimental values and recently published data of Markstein lengths for burned gases (P_i = 1 bar, τ = 0%).

At high pressure (P_i = 10 bar), the experimental values of the unstretched laminar burning velocity are less accurate because of flame cellularity effects due to hydrodynamic instabilities. This limits the number of shadowgraph images that can be used for the fitting of the flame front radius temporal evolution and so the uncertainty in the value of the unstretched laminar burning velocity is higher at these pressures. In the process of optimization of the parameters in Eq. (9), considerable weight is given to the values of laminar burning velocity at low pressure.

This can explain the discrepancies between the correlation (Eq. (9)) and the experiments at elevated pressures.

The correlations (Eqs. (6) and (9)) were finally used to predict the laminar burning velocity in the operating conditions used in the study by Kelley et al. [16]. Our correlations and their experimental results are in excellent agreement. Under the operating condition T_i = 353 K and with an air composition containing 21 vol% of O_2, the average relative error between our correlations and their experimental results is about 4%.

These global correlations can then be extrapolated to predict values of laminar burning velocity at higher pressures and temperatures and for higher dilution rates. Such conditions are

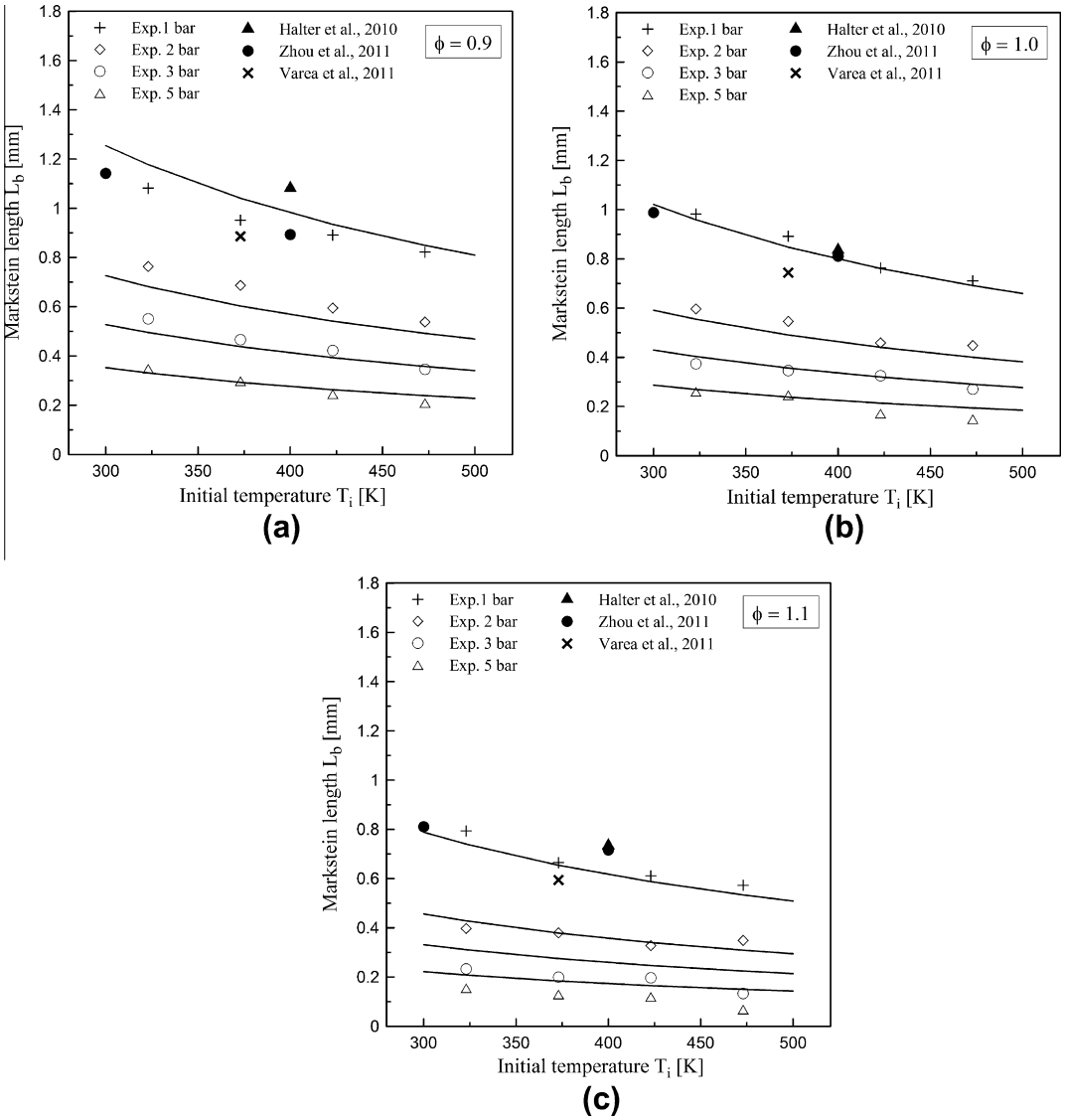

Fig. 15. Experimental Markstein length (symbols), results of the proposed correlation Eq. (10) (solid lines), and comparison with previous work [7,8,17,18] (τ = 0%).

encountered in downsized spark ignition engines. The precise prediction of flame propagation at high pressure, high temperature, and high dilution rate is essential in engine downsizing simulations.

7. Markstein lengths

The Markstein length represents the dependence of the flame propagation velocity on the stretch rate. Its value can be obtained by resolving the nonlinear Eq. (1). Experimental results have been obtained for the initial conditions reported in Tables 1 and 2. Figure 13 presents the evolution of the Markstein length for burned gases L_b versus equivalence ratio under different initial conditions. Figure 13a shows the effect of the initial temperature on the Markstein length. The influence of the initial pressure and the dilution are respectively displayed in Fig. 13b and c. Best-fit curves are plotted for clarity. The Markstein length values at $P_i = 10$ bar have not been plotted in Fig. 13b because the variation in flame velocity with stretch rate is very small, particularly at elevated pressures, so that the determination of L_b is subject to considerable uncertainty at this pressure.

In all cases, the Markstein length decreases with the increase in equivalence ratio, indicating that the propagation velocity is more sensitive to the stretch rate for lean iso-octane/air mixtures. As already observed by Zhou et al. [18], the Markstein length becomes negative at an equivalence ratio between 1.3 and 1.4, as the flame becomes unstable.

Comparisons with recent published experimental data [7,8,17,18] at atmospheric pressure are given in Fig. 14. Excellent agreement is obtained with the results of Halter et al. [8], Zhou et al. [18], and Varea et al. [17]. As already noted in a previous study [8], the Markstein lengths determined by Bradley et al. [7], using the linear methodology, are significantly greater than our results at lean equivalence ratios.

As previously done for the laminar burning velocities S_L^0, an empirical correlation is proposed to describe the Markstein length for burned gases as a function of initial temperature and pressure. This correlation is established from experimental data at equivalence ratios between 0.9 and 1.1. This range of equivalence ratios corresponds to the operating conditions of downsized spark ignition engines. In addition, the experimental Markstein lengths at these equivalence ratios are more reliable (uncertainties lower than 4%) than experimental values obtained for richer mixtures. Indeed, in the case of rich mixtures, the standard deviation, corresponding to the scattering in experiments, is higher because of flame instabilities.

The following relationship is then proposed:

$$L_b = L_{b_{\mathrm{ref}}} \left(\frac{T_i}{T_{\mathrm{ref}}}\right)^{\alpha_L} \left(\frac{P_i}{P_{\mathrm{ref}}}\right)^{\beta_L} \tag{10}$$

where

$$L_{b_{\mathrm{ref}}} = M\phi + \mathrm{N} \quad \text{with } 0.9 < \phi < 1.1 \tag{11}$$

$L_{b_{\mathrm{ref}}}$ is the value of the Markstein length under the operating conditions T_{ref} and P_{ref} (the evolution of $L_{b_{\mathrm{ref}}}$ with the equivalence ratio ϕ is linear in the range of equivalence ratios considered here). M, N, α_L and β_L are constant parameters. In this correlation, pressures P_i and P_{ref} are expressed in bar, temperatures T_i and T_{ref} in K, and Markstein lengths L_b and $L_{b_{\mathrm{ref}}}$ in mm.

All the parameters M, N, α_L, and β_L were optimized using the SSE method (minimization of the sum of squared errors). Optimized values are reported in Table 5. Figure 15 displays the results of this new correlation at equivalence ratios of 0.9, 1.0, and 1.1.

Excellent agreement is observed between calculated Markstein lengths and experimental values. The average relative error between experimental data and this correlation is lower than 15%. The maximum relative error is obtained for the conditions $P_i = 5$ bar and $T_i = 473$ K, where flame instability becomes significant.

Comparisons with previous work are added in Fig. 15. Very good agreement is obtained with the experimental results of Halter et al. [8], Zhou et al. [18], and Varea et al. [17] at atmospheric pressure.

This correlation between the Markstein length and the initial thermodynamic conditions aims at informing on the flame response to stretch. This information could be relevant to better understanding flame propagation in a real gasoline engine.

8. Conclusions

The current work addresses the need for correlations of premixed iso-octane laminar burning velocities under the highly dilute, high-initial-pressure and -temperature conditions in downsized combustion engines.

New experimental results were obtained for the laminar combustion of iso-octane/air mixtures, extending the range of previous studies. In the present work, laminar burning velocities were measured using the spherically expanding flame technique in a constant-volume chamber over a range of initial pressures ($P_i = 1$ bar – 10 bar), initial temperatures ($T_i = 323$ K – 473 K), and a wide range of equivalence ratios. An explicit correlation allowing the prediction of the laminar burning velocity, over a wide range of temperatures, pressures, equivalence ratios, and dilution rates has been proposed. Excellent agreement has been observed with recently published experimental data. Comparisons between experimental and numerical results and discrepancies between Hasse's and Jerzembeck's mechanisms confirm that iso-octane/air kinetic schemes must still be improved. The importance of the composition of air in the experimental determination of laminar burning velocities, as well as in numerical simulations, has also been highlighted.

Dilution effects, using nitrogen as diluent, and oxygen enrichment effects have also been investigated. New empirical correlations of the laminar burning velocity have been proposed and validated using numerous recent experimental results.

Finally, an empirical relationship is proposed to describe the Markstein length for burned gases as a function of initial temperature and pressure, at equivalence ratios between 0.9 and 1.1, which has never yet been done in the literature. Excellent agreement has been obtained with recently published experimental values of Markstein lengths.

Acknowledgments

This work was cofinanced by the European Union and the European Regional Development Fund. It was supported by the ICAM-DAC project through a Grant from the French National Research Agency (ANR), VTT program, Grant ANR-10-VPTT-0002.

Appendix A. Supplementary material

Supplementary data associated with this article can be found, in the online version, at http://dx.doi.org/10.1016/j.combustflame.2012.06.008.

References

[1] M.J. Atkins, et al., A Well-to-Wheel Comparison of Several Powertrain Technologies, SAE Paper, 2003-01-0081, 2003.
[2] W. Bandel, et al., The Turbocharged GDI Engine: Boosted Synergies for High Fuel Economy Plus Ultra-low Emission, SAE Paper, 2006-01-1266, 2006.
[3] M. Metghalchi et al., Combust. Flame 48 (1982) 191–210.
[4] Ö.L. Gülder, Combust. Flame 56 (1984) 261–268.
[5] S. Jerzembeck et al., Combust. Flame 156 (2009) 292–301.

[6] A.P. Kelley et al., Combust. Flame 156 (2009) 1844–1851.
[7] D. Bradley et al., Combust. Flame 115 (1998) 126–144.
[8] F. Halter et al., Combust. Flame 157 (2010) 1825–1832.
[9] R.A. Strehlow et al., Combust. Flame 31 (1978) 209–211.
[10] R.J. Kee, et al., Chemkin-II: A Fortran Chemical Kinetics Package for the Analysis of Gas Phase Chemical Kinetics, Report No. SAND89-8009B, Sandia National Laboratories, 1989.
[11] C. Hasse et al., Combust. Flame 122 (2000) 117–129.
[12] D.G. Goodwin, Cantera code site, <code.google.code/p/cantera>.
[13] H. Pitsch et al., Symp. Int. Combust. 26 (1996) 763–771.
[14] I. Glassman, Combustion, third ed., Academic Press, San Diego, CA, 1996.
[15] C. Ternel, Contribution au développement de l'allumage par laser pour les moteurs à combustion interne, Thèse de doctorat, Université de Rouen, 2006.
[16] A.P. Kelley et al., Proc. Combust. Inst. 33 (2011) 501–508.
[17] E. Varea et al., Combust. Flame (2011).
[18] J.X. Zhou et al., Combust. Flame 158 (2011) 2375–2383.
[19] G. Broustail, Potentiel de l'utilisation des mélanges hydrocarbures/alcools pour les moteurs à allumage commandé (Potential of hydrocarbons/alcohols blends use in spark-ignition engines), Thèse de doctorat, Université d'Orléans, 2011.
[20] V.S. Babkin et al., Combust. Explos. Shock Waves 3 (1967) 221–225.
[21] S.P. Marshall et al., Combust. Flame 158 (2011) 1920–1932.
[22] J.B. Martz et al., Combust. Flame 158 (2011) 1089–1096.
[23] U.C. Müller et al., Combust. Flame 108 (1997) 349–356.
[24] T. Tahtouh, Les effets combinés de l'hydrogène et de la dilution dans un moteur à allumage commandé (Combined effects of hydrogen and dilution in a spark ignition engine), Thèse de doctorat, Université d'Orléans, 2010.
[25] S.G. Davis et al., Symp. Int. Combust. 27 (1998) 521–527.
[26] J.E. Freeh, et al., Laminar flame speeds of preheated iso-octnae/air and n-decane/air flames using digital particle image velocimetry, in: 40th AIAA/ASME/SAE/ASEE Joint Propulsion Conference and Exhibit, 2004-3709, 2004.
[27] Y. Huang et al., Combust. Flame 139 (2004) 239–251.
[28] K. Kumar et al., J. Propuls. Power 23 (2007) 428–436.
[29] J.P.J. Lipzig et al., Fuel 90 (2011) 2773–2781.
[30] C. Mandilas et al., Proc. Combust. Inst. 31 (2007) 1443–1450.